A structural framework for interpretation of four-electrode microimpedance spectra in cardiac tissue

Andrew E. Pollard[1] and Roger C. Barr[2]

Abstract— **Renewed interest in the four-electrode method for identification of passive electrical properties in cardiac tissue has been sparked by a recognition that measurements made with sensors in close proximity are frequency dependent. Therefore, resolution of four-electrode microimpedance spectra (4EMS) may provide an opportunity for routine identification of passive electrical properties for the interstitial and intracellular compartments using only interstitial access. The present study documents a structural framework in which the tissue resistivity (ρ_t) and reactivity (χ_t) that comprise spectra are computed using interstitial and intracellular microimpedance distributions that account for differences in compartment size, anisotropic electrical properties in each compartment and electrode separations. We used this framework to consider 4EMS development with relatively wide (d=1 mm) and fine (d=250 μm) electrode separations and sensors oriented along myocyte axes, across myocyte axes and intermediate between those axes.**

I. INTRODUCTION

In total tissue resistivity (ρ_t) experiments with heart preparations [1], [2], [3], [4], a four-electrode configuration is often used with delivery of supplied current to the interstitial compartment via two outer stimulating electrodes establishing an interstitial potential field that is monitored by two inner voltage-sensing electrodes. Calibration is important in such experiments, as ρ_t is derived from the ratio between the central potential difference (uPD) and the supplied current (Istim) after uPD/Istim is scaled by a probe constant (Kp). Kp, which is identified in advance of electrophysiologic study during stimulation and recording with a solution of known conductivity (ρ_k), is intended to account for variations between the expected and measured ratio due to inconsistencies in electrode positions and to contributions of electrode-electrolyte interfaces at each sensor. Although ρ_t depends upon the passive electrical properties of the intracellular and interstitial compartments as well as on membrane resistance and capacitance, measurements are usually made during DC stimulation or AC stimulation at a single frequency. One might anticipate use of multiple frequencies to identify a complex composite impedance (uCI) spectra whose magnitude (|uCI|) and phase ($\angle$uCI) depend upon the tissue's complete resistive and capacitive properties would provide an opportunity to quantify component values for circuit representations of tissue near the electrodes. However, the uCI spectra changes little with frequency when traditional separations (mm size scale) are employed. This occurs because much of the supplied current crosses cell membrane separating the compartments when the spatial scale exceeds the tissue space constant [5], [6]. Equivalent current redistribution between compartments occurs at all frequencies with traditional separations.

Theory predicts that as sensors are moved closer to one another, stimulation frequency will influence compartment redistribution [5], [6]. With finer separation, total intracellular and interstitial resistance in the supplied current pathway decreases while membrane resistance increases. At sufficiently fine spacing, inability of supplied current to cross membrane at low frequency leads to increased |uCI| because supplied current remains primarily interstitial. Membrane capacitance contributes little to the low frequency response such that any phase shift between current and voltage records is small. At intermediate and high frequencies, however, capacitive shunting provides an alternate pathway for compartment redistribution, lowering |uCI| and establishing $\angle$uCI. Spectra resolution with fine spacing therefore provides an opportunity to segment interstitial from intracellular contributions to ρ_t, which to date has been achieved most often with preparations in which both interstitial and intracellular access is maintained [7]. Continuous intracellular access is technically challenging in that fragile glass microlelectrodes and specialized tissue preparations are required. Collectively, these challenges complicate routine measurements during electrophysiologic study with hearts.

The goal of the present study was to examine development of four-electrode microimpedance spectra (4EMS) in a three-dimensional structural framework whose component building blocks included constitutive interstitial (Rox,Roy,Roz), intracellular (Rix,Riy,Riz) and membrane (Rm,Cm) microimpedances with values derived from the limited data available for rabbit ventricular myocardium. Using this framework, we computed frequency-dependent |uCI| and $\angle$uCI at two interelectrode separations. The first separation was typical of that used in traditional total tissue resistivity experiments while the second approximated the size of an individual electrode used in a traditional experiment. This allowed identification of qualitative and quantitative predictions for 4EMS development that included consideration of the electrodes' orientation relative to myocyte axes.

II. METHODS

In a traditional tissue resistivity experiment, an electrode array is calibrated by placement in a weakly conducting salt solution of known resistivity in the 100-500 Ω-cm range [1],

*This work was supported by NIH award HL092049

[1]A. Pollard is with the Department Biomedical Engineering, Cardiac Rhythm Management Laboratory, University of Alabama Birmingham, Birmingham, AL, USA apollard@uab.edu

[2]R. Barr is with the Department of Biomedical Engineering, Duke University, Durham, NC, USA roger.barr@duke.edu

978-1-4244-7929-0/14/$26.00

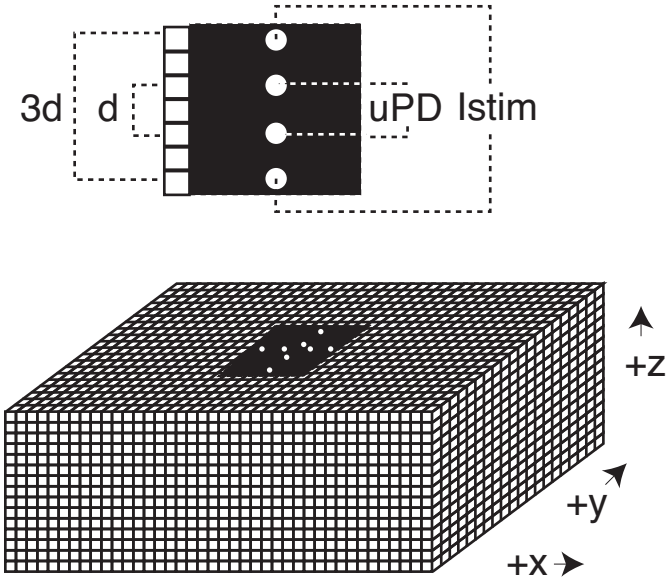

Fig. 1. Schematic diagram showing electrode separations atop three-dimensional structural framework used for passive membrane simulations. Black region includes the surface location for the electrode array. The uPD was recorded from blocks separated by d=2△. The Istim was supplied from blocks separated by 3d=6△. Electrode orientations along (x) myocyte axes, across (y) myocyte axes and on the diagonal between those axes (not shown) were considered.

[2], [3], [4], in advance of electrophysiologic study. Since no biological sources for capacitance are present in the media a probe constant is identified as Kp=ρ_k/uCI. Kp therefore has units of cm. The analytic predictions for uCI with a four-electrode arrangement including a separation between the sensors used to record uPD of d and a separation between the sensors used to supply Istim of 3d are $\rho_k/4\pi$d and $\rho_k/2\pi$d, respectively, assuming the array is positioned inside an infinite isotropic volume conductor or on the surface of a semi-infinite volume conductor. In practice, the range is used because any insulating material in which the electrodes are embedded will contribute to an intermediate uCI, as will solution that wicks around the array surface during calibration. We used Kp=2πd.

Figure 1 shows the structural framework we used to represent cardiac tissue. That framework included (40x20x15=12,000) individual building blocks in which (Rox,Roy,Roz), (Rix,Riy,Riz) and (Rm,Cm) were prescribed using macroscopic descriptions available from the literature. For the compartments, we defined

$$R_{c,s} = (\rho_c \alpha_{c,s})/(f_c \triangle) \tag{1}$$

with subscript c denoting intracellular (i) or interstitial (o) compartment, subscript s denoting direction (x,y,z), ρ compartment resistivity, f compartment volume fraction, $\triangle$ the edge length for a building block and α an anisotropy ratio. We used ρ_i=166 Ω-cm and ρ_o=63 Ω-cm [7] and aligned myocyte axes with the x-direction, $\alpha_{i,x}$, $\alpha_{i,y}$, $\alpha_{i,z}$ of 1.0, 9.4, 9.4, respectively, [8] $\alpha_{o,x}$, $\alpha_{o,y}$, $\alpha_{o,z}$ of 1.0, 2.7, 2.7, respectively, [8] and f_i, f_o of 0.8 and 0.2, respectively [10]. For the membrane, we defined

$$Rm = (R_{in} V_{cell})/\triangle^3 \tag{2}$$

and

$$Cm = (C_{cell} \triangle^3)/V_{cell} \tag{3}$$

with input resistance R_{in}=33.7 MΩ, cell capacitance C_{cell}=72.5 pF and cell volume V_{cell}=16,201 μm^3 [9].

Assigning (Rox,Roy,Roz), (Rix,Riy,Riz) and (Rm,Cm) for a given $\triangle$ allowed numerical determination of transmembrane (Vm) and interstitial (ϕ_o) potentials at all building blocks using an approach that followed our earlier report [6]. For the linear system

$$[G]\overline{v} = \overline{b} \tag{4}$$

[G] was a coefficient matrix that accounted for connections between building blocks via (Rox,Roy,Roz) and (Rix,Riy,Riz) based on total membrane current (Im)

$$Im = \sum_s \frac{\triangle Vm^{+s} - \triangle Vm^{-s} + \triangle {\phi_o}^{+s} - \triangle {\phi_o}^{-s}}{R_{i,s}} \tag{5}$$

and

$$Im = \sum_s \frac{\triangle {\phi_o}^{+s} - \triangle {\phi_o}^{-s}}{R_{o,s}} \tag{6}$$

with Eqns. (5) and (6) balanced by

$$Im = Vm \frac{Rm + Xm}{RmXm} \quad . \tag{7}$$

In Eqn. (7), membrane reactance (Xm=j/ωCm) depends upon $j = \sqrt{-1}$ and angular frequency (ω). In this form, $\overline{v}$ was a vector of unknown potentials shose lower half contained Vm values and whose upper half contained ϕ_o values, and $\overline{b}$ was a source vector whose lower half depended upon Eqn. (7) and whose upper half was set to zero except at blocks where current sources or sinks were located. Because [G] was assembled using the MATLAB (MathWorks, Natick, MA) sparse matrix function, solutions for $\overline{v}$ were readily achieved using the GMRES function with incomplete Cholesky preconditioning to accelerate solutions over a range of frequencies from 1 Hz to 100 kHz. Source (+1 μA) and sink (-1 μA) building blocks were oriented along myocyte axes, across myocyte axes and on the diagonal between myocyte axes in different simulations. and uPDs were acquired from the difference in ϕ_o between associated inner blocks separated by d=2△. Inclusion of Xm ensured identification of |uCI| and ∠uCI.

In each simulation, we then identified

$$\rho_t = Kp|uCI|cos(\angle uCI) \tag{8}$$

with

$$\chi_t = Kp|uCI|sin(\angle uCI) \tag{9}$$

and the fraction of total supplied current (Ii) that passed through the intracellular compartment between the building blocks from which uPD was recorded. Identifying the 4EMS in terms of ρ_t and χ_t was advantageous in practice because spectra were normalized for comparisons between different electrode separations with both terms having units of Ω-cm. Identifying Ii allowed assessment of the extent to which supplied current redistributed intracellularly for each frequency, electrode separation and electrode orientation.

III. RESULTS

When the electrodes were oriented across myocyte axes, the frequency-dependent 4EMS that developed with a separation of d=250 μm was much more pronounced than the 4EMS that developed with a separation of d=1 mm. Figure 2a shows ρ_t and χ_t for these two spectra. With d=250 μm, ρ_t fell from a maximum of 376 Ω-cm in the 1-10 Hz band to a minimum of 264 Ω-cm in the 1.5-100 kHz band such that the overall ρ_t range was 112 Ω-cm. A substantive reactive component was also observed, as we found χ_t rose to 106 Ω-cm at 100 Hz. Frequencies at which χ_t measured less than 20 Ω-cm included the 1-10 Hz and 4-100 kHz bands. With d=1 mm, evidence of 4EMS development was much less pronounced as the ρ_t range was only 15 Ω-cm and maximal χ_t was limited to 3 Ω-cm at 100 Hz. A paired t-test including all 4EMS parameters showed a statistically significant ($p \leq 0.05$) difference between populations assembled using all samples at each separation. That difference was not significant when populations were limited to samples from the 1-100 kHz band. When the electrodes were oriented on the diagonal intermediate to the main axes, qualitative features of 4EMS development were maintained as there was much more limited spectra development with d=1 mm than with d=250 μm and overall frequency dependence with d=250 μm included ρ_t that fell over an intermediate band as χ_t increased. Quantitative differences from the 4EMS with electrodes oriented across myocyte axes included a wider ρ_t range at 144 Ω-cm, a larger maximal χ_t of 176 Ω-cm, and a shift to 175 Hz for maximal χ_t.

By comparison, there were both qualitative and quantitative differences in 4EMS development with d=250 μm when the electrodes were oriented along the myocyte axes. First, ρ_t fell from a maximum of 633 Ω-cm in the 1-10 Hz band to a minimum of 319 Ω-cm at 300 Hz and then rose to 479 Ω-cm by 10 kHz, which was the value maintained at frequencies up to 100 kHz. The ρ_t range was not only wider at 314 Ω-cm, but the rise in ρ_t in the 0.3-10 kHz band was a 4EMS feature that was less apparent with the other electrode orientations. Second, χ_t rose to 382 Ω-cm at 175 Hz before falling to a minima of -127 Ω-cm at 2 kHz. That minima was followed by a subsequent return to less than -20 Ω-cm win 20-100 kHz band. The 1-10 kHz band in which χ_t was below -20 Ω-cm was unique to this electrode orientation. Finally, χ_t exceeded ρ_t in the 150-300 Hz band.

An alternate way in which the different 4EMS from Figure 2 can be considered is through comparisons between the fraction of supplied current that flowed through

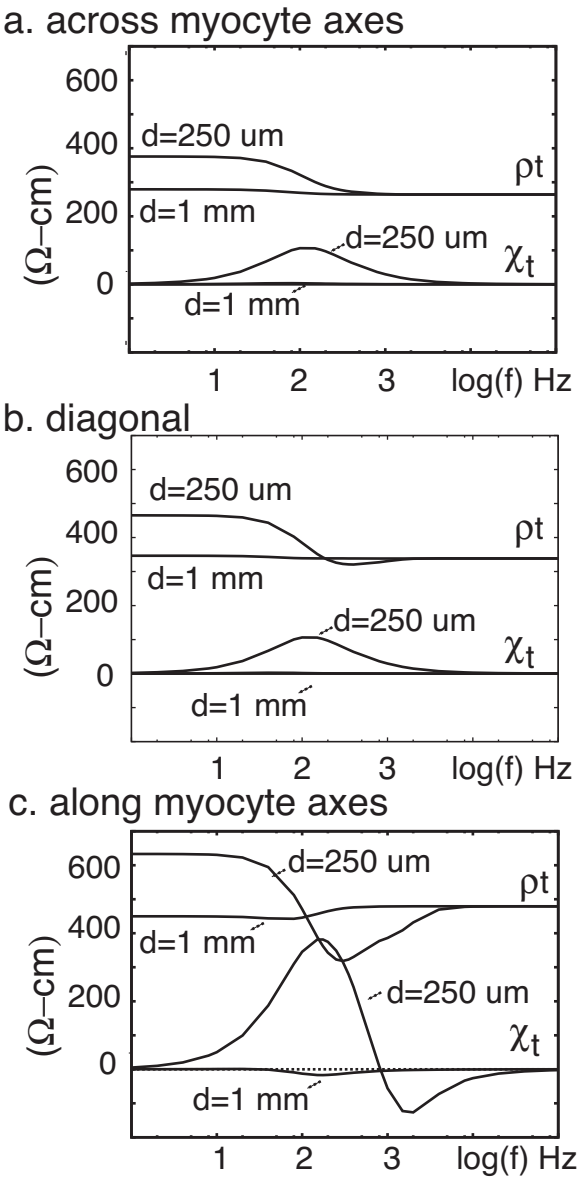

Fig. 2. Impedance spectra from passive membrane simulations with electrodes oriented (a) across myocyte axes (b) on the diagonal between axes and (c) along myocyte axes.

the intracellular compartment in the measurement region for the electrode separations and orientations we analyzed. Figure 3 shows Ii for both electrode separations. With 1 mm separation, the main differences in Ii were in the fractions themselves. As electrode orientation shifted off the myocyte axes, Ii decreased. This occurred because the prescribed Riy was 9.4-fold higher than the prescribed Rix and the prescribed Roy was 2.7-fold higher than the prescribed Rox. As such, Vm and ϕ_o reductions near the stimulating electrodes were most pronounced with electrodes oriented across myocyte axes with the supplied current being shunted into building blocks off the measurement axis. The same general features were observed with d=250 μm in the high frequency bands from our simulations. At relatively low frequencies, however, Ii differences between the 3 electrode

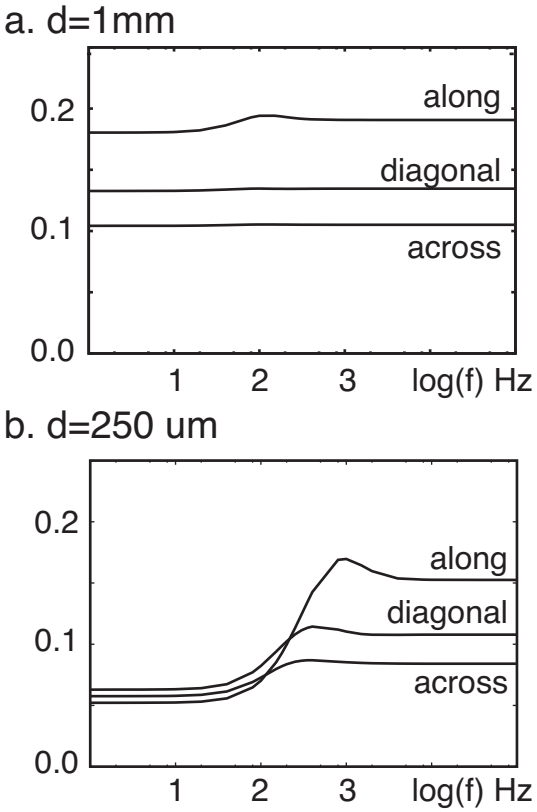

Fig. 3. Fraction of supplied current that crossed membrane and passed through the building blocks from which uPDs were recorded with (a) d=1mm and (b) d=250 μm.

orientations were relatively small. This occurred because supplied current remained primarily interstitial as only ≈5% of that current redistributed to the intracellular compartment in the central building blocks. Supplied current that reached the intracellular compartment in the measurement region was influenced by the differences between Roy and Rox to a greater extent than the differences between Riy and Rix. At intermediate frequencies, development of negative χ_t accelerated redistribution of supplied current to the intracellular compartment. This effect was most pronounced with electrodes oriented along myocyte axes.

IV. DISCUSSION

Along with precise fabrication of electrode sets, a major hidden technical challenge to experimental assessment of 4EMS involves the relatively high electrode-electrolyte impedances associated with the very small sensors necessary to achieve fine separations. With small electrodes, amplifier inputs for voltage sensing may not function as open circuits because each electrode-amplifier interconnection has the potential to establish a capacitive shunt to system ground that depends upon the electrode-electrolyte impedance [12]. Parasitic capacitance in the measurement system may then influence the spectra in ways that complicate segmentation of the tissue's influence on the spectra from the instrumentation's influence on the spectra. This issue is more managable when larger electrodes are employed. Most investigators who have completed four-electrode measurements with whole heart preparations have used arrays with 250 μm to 1 mm diameter electrodes separated on a mm to cm size scale. Although arrangements of this type limit the instrumentation's influence, spectra do not develop with traditional separations because Istim redistribution is equivalent at all frequencies, consistent with predictions for 4EMS here using d=1 mm.

In a recent report [11], we documented the characteristics of a measurement approach that we anticipate will allow assessment of predictions of this structural framework using d=250 μm. With that system, voltages at all electrodes are sensed with a head stage that eliminates DC offsets, establishes an active shield signal for each sensor, and generates a driven common signal supplied to the tissue bath. Collectively, these features limit the instrumentation's influence on the spectra. Signals necessary for both $|\text{uCI}|$ and $\angle\text{uCI}$ are digitized at high sampling rate and resolution for rapid reconstruction of 4EMS. We therefore believe adaptation to resolve 4EMS with fine interelectrode separation and careful positioning of arrays in regions of cardiac tissue where myocardial structure can be resolved is practical to achieve.

REFERENCES

[1] Tsai JZ, Will JA, Hubbard Van Stelle S, Cao H, Tungjitkusolmun S, Choy YB, Haemmerich D, Vorperian VR, and Webster JG. In-vivo measurement of swine myocardial resistivity. *IEEE Trans Biomed Eng.*, 49:472–483, 2002.

[2] Rodriguez-Sinovas A, Garcia-Dorado D, Ruiz-Meana M, and Soler-Soler J. Enhanced effect of gap junction uncouplers on macroscopic electrical properties of reperfused myocardium. *J. Physiol.*, 559:245–257, 2004.

[3] Steendijk P, van der Velde T, and Baan J. Dependence of anisotropic myocardial electrical resistivity on cardiac phase and excitation frequency. *Basic Res. Cardiol.*, 89:411–426, 1994.

[4] Dumas JH, Himel HD, Kiser AC, Quint SR, and Knisley SB. Myocardial electrical impedance as a predictor of the quality of rf-induced linear lesions. *Physiol. Meas.*, 29:1195–1207, 2008.

[5] Roth, BJ, Gielen, FLH, and Wikswo, JP. Spatial and temporal frequency-dependent conductivities in volume-conductor calculations for skeletal muscle. *Math. Biosci.* 88:159–189, 1988.

[6] Pollard AE and Barr RC. A biophysical model for cardiac microimpedance measurements. *Am. J. Physiol. Heart Circ. Physiol.*, 298:H1699–H1709, 2010.

[7] Kléber AG and Rieger CB. Electrical constants of arterially perfused rabbit papillary muscle. *J. Physiol. (London)*, 385:307–324, 1987.

[8] Clerc, L. Directional differences of impulse spread in trabecular muscle from mammalian heart. *J. Physiol. (London)* 255:335–346, 1976.

[9] Giles, WR and Imaizumi, Y. Comparison of potassium currents in rabbit atrial and ventricular cells. *J. Physiol. (London)* 405:123–145, 1988.

[10] Polimeni, PI, Williams, S, and Weisman, H. Application of automatic electronic image analyzer to the measurement of myocardial extracellular space. *Comp. Biomed. Res.* 16:522, 1983.

[11] Pollard, AE and Barr, RC. A new approach for resolution of complex tissue impedance spectra in hearts. *IEEE Trans. Biomed. Eng.* 60:2494–2503, 2013.

[12] Mazzeo, BA. Parasitic capacitance influence of potential-sensing electrodes on four-electrode liquid impedance measurements. *J. Appl. Phys.* 105:0941061–0941065, 2009.